remote sensing

MDPI

Supplementary Information to

High-Spatial Resolution Monitoring of Phycocyanin and Chlorophyll-a using Airborne Hyperspectral Imagery

JongCheol Pyo[1], Mayzonee Ligaray[1], Yong Sung Kwon[1], Myoung-Hwan Ahn[2], Kyunghyun Kim[3], Hyuk Lee[4], Taegu Kang[4], Seong Been Cho[5], Yongeun Park[6*] and Kyung Hwa Cho[1*]

[1] School of Urban and Environmental Engineering, Ulsan National Institute of Science and Technology, Ulsan, 689-798, Republic of Korea; jcp01@unist.ac.kr (J.C.P.); mayzonee@gmail.com (M. L.); wizkys@unist.ac.kr (Y.S.K.); khcho@unist.ac.kr (K.H.C.)

[2] Department of Atmospheric Science and Engineering, Ewha Womans University, Ewha-Yeodae-Gil 52, Seodaemoon-Gu, Seoul, Republic of Korea; terryahn65@gmail.com (M.H.A.)

[3] Yeongsan River Environmental Research Center, National Institute of Environmental Research, Gwangju, 61011, Republic of Korea; matthias@korea.kr (K.K.)

[4] Water Quality Assessment Research Division, National Institute of Environmental Research, Environmental Research Complex, Incheon, 22689, Republic of Korea; ehyuk72@korea.kr (H. L.); taegu98@korea.kr (T.K.)

[5] GEOSTROY Inc., Hwa-gok-lo 68-82, Gangseo-Gu, Seoul, Republic of Korea; losttemple85@geostory.co.kr (S.B.C)

[6] School of Civil and Environmental Engineering, Konkuk University, Neumgdong-Ro 120, Gangjin-Gu, Seoul, Republic of Korea; yepark@konkuk.ac.kr (Y.P.)

* Co-Correspondence khcho@unist.ac.kr (K.H.C.); yepark@konkuk.ac.kr (Y.P.); Tel.: +82-052-217-2829

A manuscript for

Remote Sensing

Appendix A. Atmospheric Correction of ATCOR 4, MODTRAN 6, and ANN

A1. ATCOR 4

ATCOR 4 is based on the MODTRAN 4 code that calculates the radiative transfer function and provides the physical parameterization using in-situ reflectance and metrological data [1]. In this study, the ATCOR library for atmospheric conditions was used, and the Lambertian surface was set. The ATCOR 4 was then run to generate modeled reflectance using Eq. (S1),

$$\rho_{\mathrm{surf}} = \frac{\pi(\mathrm{D}^2\mathrm{L}_{\mathrm{at-sensor}} - \mathrm{L}_{\mathrm{path}})}{\mathrm{TF}_{\mathrm{g}}} \quad \text{(S1)}$$

where, ρ_{surf} is the surface reflectance (sr^{-1}), D^2 is the sun-to-earth distance (astronomical unit), $L_{at-sensor}$ is the total radiance through the sensor (mW cm^{-2} sr^{-1} μm^{-1}), $\mathrm{L}_{\mathrm{path}}$ is the atmospheric path radiance (mW cm^{-2} sr^{-1} μm^{-1}), T is the atmospheric transmittance, and F_{g} is the global flux on the ground (mW cm^{-2} μm^{-1}).

A2. MODTRAN 6

MODTRAN was developed by Spectral Science, Inc. and the Air Force Research Laboratory (AFRL) [2]. The MODTRAN code solves the radiative transfer function to generate physical parameters related to atmospheric correction such as transmittance and spherical albedo. MODTRAN version 6 has a graphical user interface (GUI), making this software user-friendly

The MODTRAN 6 inputs were built to generate atmospheric correction parameters for the Baekje Weir (Table S1). The statistical band model and discrete ordinate radiative transfer were selected as the radiative transfer and multiple scattering algorithms, respectively. A mid-latitude summer atmospheric profile was used and the CO_2 concentration was set to 400 ppmv. The rural boundary layer aerosol option was selected. The geometry was specified by selecting the solar zenith angle and solar azimuth angle according to the date the field data were collected (Table S2). This geometry was then used to set the solar geometry specification parameters for solar scattering. The zenith angle of the hyperspectral sensor was set to 180 degrees since the sensor was installed on an aircraft perpendicular to the ground. Information on monitoring time and geographic coordinates (i.e., latitude and longitude) for each sampling point were written in the geometry input section. Lambertian spectral reflectance was defined in the surface specification option. The spectral specification option set the spectral range of the MODTRAN output from 400 nm to 800 nm. The MODTRAN 6 output provided atmospheric correction parameters such as atmospheric path radiance, total solar flux, direct transmittance, diffuse transmittance, and spherical albedo. Based on simulated atmospheric correction parameters, the radiometric calibration converting from digital number (DN) of the raw hyperspectral image to at-sensor radiance was done following [3]. ρ_{surf} was calculated by inverting the radiometric calibration equation:

$$\rho_{\mathrm{surf}} = \frac{\pi(\mathrm{L}_{\mathrm{at-sensor}} - \mathrm{L}_{\mathrm{path}})}{\pi(\mathrm{L}_{\mathrm{at-sensor}} - \mathrm{L}_{\mathrm{path}})\mathrm{S} + \mathrm{TF}_{T}} \quad \text{(S2)}$$

where ρ_{surf} is the surface reflectance (sr^{-1}), $L_{at-sensor}$ is the total radiance through the sensor ($Wcm^{-2}sr^{-1}cm^{-1}$), $\mathrm{L}_{\mathrm{path}}$ is the atmospheric path radiance ($Wcm^{-2}sr^{-1}cm^{-1}$), S is the spherical albedo of the atmosphere, T is the atmospheric transmittance, and F_{T} is the total solar flux at the ground ($Wcm^{-2}cm^{-1}$). The average value of calibrated radiative parameters was distributed on the hyperspectral image to calculate ρ_{surf} pixel-by-pixel.

A3. ANN for Atmospheric Correction

The ANN model was composed of an input layer, a hidden layer, and an output layer. Each layer has nodes, which were connected to the nodes in other layers by transfer functions and a backpropagation function. The input layer included the atmospheric correction parameters (i.e. atmospheric path radiance, total solar flux at the ground, direct transmittance, diffuse transmittance, and spherical albedo) obtained from the MODTRAN 6 simulation and image DN. The number of nodes in a hidden layer, the network parameters (i.e. learning rate and momentum constant), the transfer functions, and the backpropagation function were optimized using a pattern search algorithm ([4] Park et al 2017). The output layer consisted of in-situ reflectance. This study selected the reflectance of 12 bands as input data since the reflectance is related to PC and Chl-a estimation by the bio-optical algorithms (Table S3). A total of 888 input data points was obtained from the four monitoring campaigns; 77% of the data (688 data points) were used to train the ANN model, and 23% of the data (200 data points) were used to validate the model. An ANN model was built to simulate surface reflectance using atmospheric correction parameters at specific wavelength bands (Table S3). The ANN model consisted of five layers: an input layer, three hidden layers, and an output layer. A pattern search algorithm was used to optimize the network parameters of the ANN model. The network parameters included the optimal number of nodes, the transfer function, the learning rate, and the momentum constant. A total of 10,000 iterations were used. The optimized number of hidden nodes in the first, second, and final layers were five nodes, four nodes, and one node, respectively. The ANN model uses a tangent sigmoid function to transfer the signals between layers; the tangent sigmoid function was chosen over the linear and log sigmoid functions by trial and error. The backpropagation network training function was set to 'trainlm', which is a Levenberg-Marquardt backpropagation . The optimized learning rate and momentum constant were 0.13 and 0.97, respectively. The NSE values of the optimized ANN model were 0.80 for the training step and 0.76 for the validation step.

Table S1. MODTRAN input composition

MODTRAN input	Input parameter	Description
Radiative transfer input	RT_MODTRAN	MODTRAN statistical band model algorithm
	RT_DISORT_OBS	Discrete ordinate multiple scattering algorithm
Atmosphere specific input	ATM_MIDLAT_SUMMER	Mid-latitude summer
	CO2MX	CO_2 concentration as 400 ppmv
Aerosol specific input	AER_RURAL	Rural boundary layer of aerosol
Geometric specific input	OBSZEN	Zenith angle of sensor as 180°
	SA	Solar azimuth angle (see Table 3)
	SZ	Solar zenith angle (see Table 3)
Surface specific input	REFL_LAMBER_MODEL	Lambertian spectral reflectance
Spectral specific input	Spectral bandpass(V1-V2)	Spectral range as 400nm-800nm

Table S2. Solar angle for geometry specific input.

	08.12.2016		08.24.2016		09.20.2016		10.14.2016	
Image section	**SZ***	**SA****	**SZ**	**SA**	**SZ**	**SA**	**SZ**	**SA**
1	52.6	99.3	25.6	171.9	44.8	135.3	43.6	162.1
2	54.7	97.0	41.8	117.8	45.8	133.2	44.6	159.9
3	53.5	97.8	42.6	116.7	46.7	131.4	47.0	158.3

* and ** indicate solar zenith angle and solar azimuth angle with unit as degree (°).

Table S3. Input information for the ANN.

Parameter	Band	Algorithm
Direct transmittance	439nm	IOP algorithm
	443nm	IOP algorithm
Diffuse transmittance	534nm	IOP algorithm
	599nm	IOP algorithm
Total solar flux	618nm	IOP algorithm
	622nm	IOP and AOP algorithm
Atmospheric path radiance	627nm	IOP algorithm
	660nm	IOP algorithm
Spherical albedo	674nm	IOP algorithm
	708nm	IOP and AOP algorithm
Digital number	755nm	AOP algorithm
	779nm	IOP algorithm

Table S4. Atmospheric correction performances of MODTRAN 6 and ATCOR 4. NSE = Nash-Sutcliffe Efficiency.

	MODTRAN 6							
	08.12.2016		08.24.2016		09.20.2016		10.14.2016	
Point	**NSE**	**RMSE***	**NSE**	**RMSE**	**NSE**	**RMSE**	**NSE**	**RMSE**
1	0.48	0.0025	1.00	0.00013	0.96	0.00052	0.95	0.00058
2	0.43	0.0020	0.95	0.00072	0.98	0.00035	0.13	0.0015
3	0.92	0.0015	0.94	0.00072	0.97	0.00041	-0.13	0.0018
4	0.98	0.00035	0.72	0.0016	0.97	0.00035	0.88	0.00069
5	1.00	0.00016	0.92	0.00083	0.98	0.00031	0.47	0.0012
6	0.98	0.00026	0.89	0.0010	0.99	0.00026	0.87	0.00067
7	0.41	0.0015	0.86	0.0011	0.97	0.00049	0.91	0.00080
8	0.86	0.00081	0.89	0.0011	0.98	0.00029	0.89	0.00058
9	0.81	0.00072	0.99	0.00024	0.93	0.00058	0.87	0.00057
10	0.83	0.00077	0.97	0.00049	0.97	0.00036	0.84	0.00067
11	0.82	0.00090	0.98	0.00039	0.84	0.00076	0.16	0.0012
12	0.93	0.00056	1.00	0.00016	0.87	0.00075	0.40	0.0017
13	0.84	0.00078	0.67	0.0015	0.97	0.00039	-1.67	0.0023
14	0.92	0.00075	0.86	0.0012	0.96	0.00049	-0.50	0.0019
15	0.92	0.00063	0.98	0.00043	0.96	0.00043	0.01	0.0017
16	1.00	0.000090	0.75	0.0012	0.93	0.00059	0.81	0.0012
17	0.99	0.00019	0.81	0.0012	0.92	0.00069	-1.38	0.0022
18	0.99	0.00014	0.94	0.00081	-	-	0.66	0.0012
19	-	-	0.96	0.00055	-	-	-1.95	0.0025
20	-	-	-	-	-	-	-1.09	0.0034
	ATCOR 4							
Point	**NSE**	**RMSE**	**NSE**	**RMSE**	**NSE**	**RMSE**	**NSE**	**RMSE**
1	-5.27	0.0086	-13.71	0.010	10.70	0.0088	-3.75	0.0057
2	-4.97	0.0064	-16.91	0.013	-5.10	0.0060	-6.61	0.0045
3	-6.15	0.015	-11.80	0.011	-4.59	0.0055	-14.59	0.0068
4	-14.20	0.0086	-19.45	0.013	10.11	0.0065	-5.19	0.0050
5	-9.85	0.0080	-10.98	0.0099	-3.27	0.0049	-3.17	0.0034
6	-11.50	0.0064	-8.15	0.0094	-5.68	0.0059	-8.47	0.0058
7	-8.66	0.0059	-6.97	0.0084	-4.68	0.0070	-6.32	0.0074
8	-9.13	0.0070	-9.33	0.010	-4.91	0.0052	-8.60	0.0055
9	-10.12	0.0055	-8.91	0.0078	-4.71	0.0053	-8.28	0.0049
10	-7.70	0.0055	-9.64	0.0091	-7.15	0.0061	-14.69	0.0067
11	-13.49	0.0080	-9.88	0.0092	-6.76	0.0052	-9.30	0.0044
12	-7.01	0.0062	-10.06	0.0090	-7.89	0.0062	-10.66	0.0076
13	-13.76	0.0076	-13.32	0.0099	-7.99	0.0062	-22.36	0.0067
14	-9.50	0.0086	-13.82	0.012	-6.35	0.0064	-1.38	0.0024
15	-11.86	0.0080	-14.66	0.012	-8.16	0.0068	-8.68	0.0054
16	-10.39	0.0069	-20.28	0.011	-5.73	0.0058	-10.48	0.0091
17	-8.59	0.0063	-24.82	0.013	-6.70	0.0068	-1.71	0.0024
18	-8.12	0.0056	-14.72	0.014	-	-	-8.71	0.0065
19	-	-	-17.77	0.012	-	-	-2.96	0.0029

20	-	-	-	-	-	-	-10.84	0.0080

*Unit of RMSE is sr^{-1}

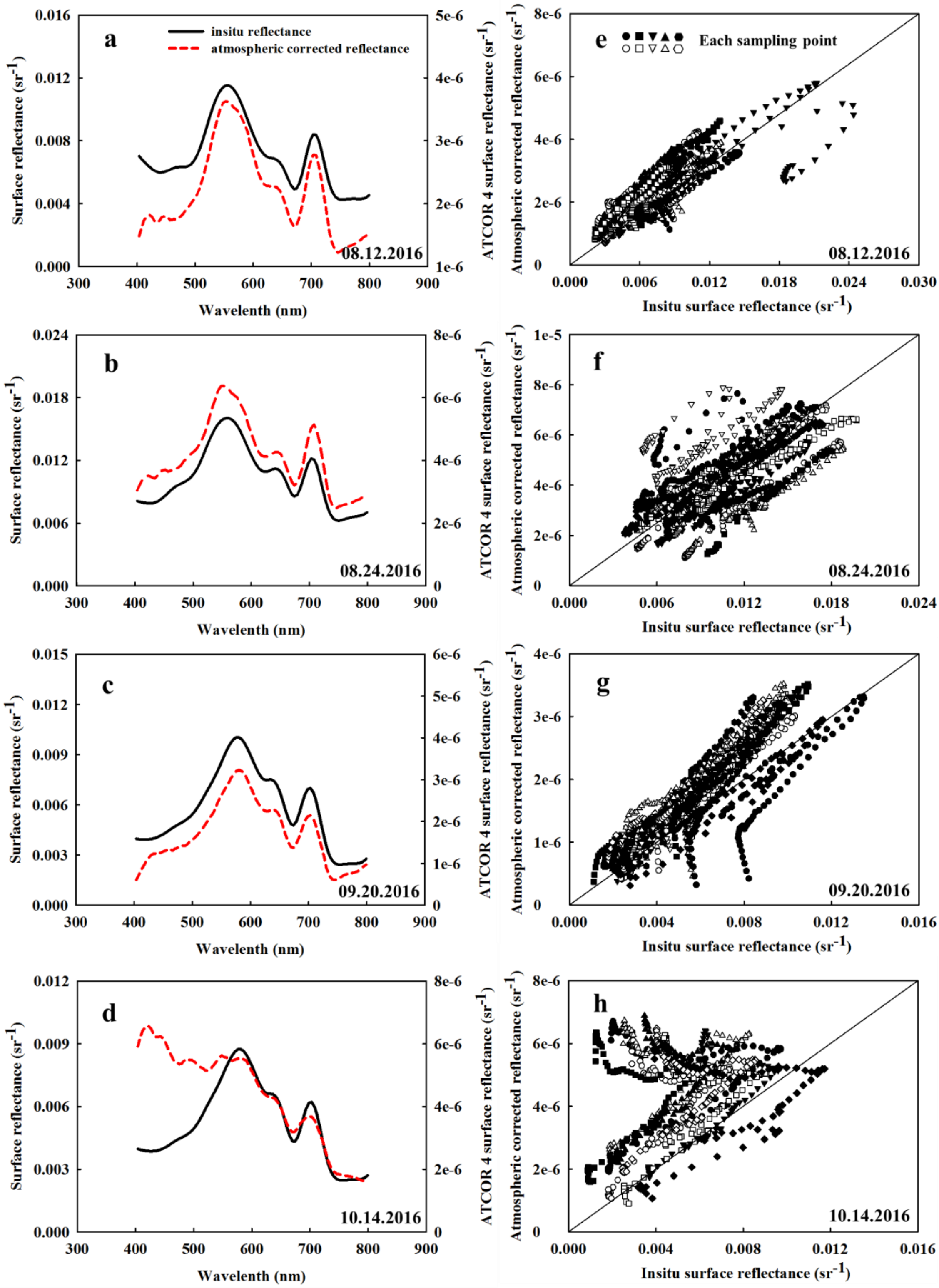

Fig. S1 Atmospheric correction results using ATCOR 4. Panels **a-d** show the average in-situ and corrected surface reflectance ρ_{surf}. Panels **e–h** show the correlation between the observed and corrected results at different wavelengths for each sampling point.

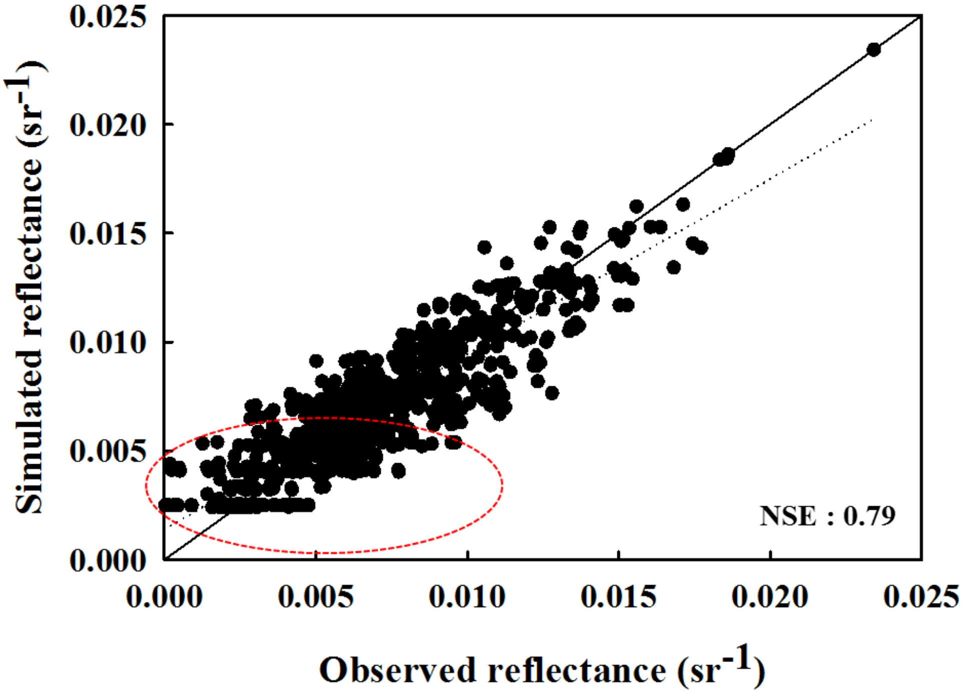

Fig. S2 ANN simulation of atmospheric correction results for overall wavelengths.

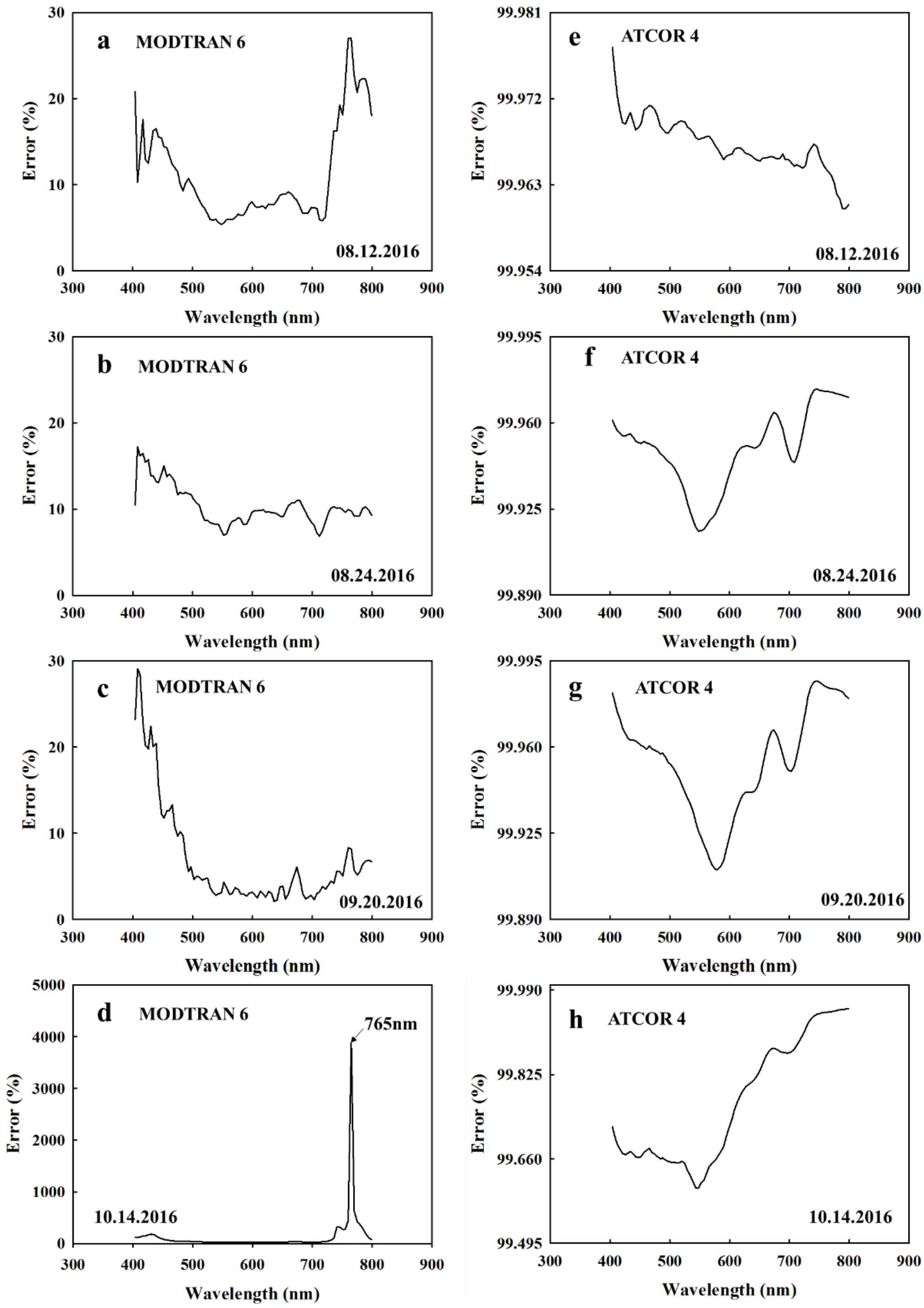

Fig. S3 Reflectance error (%) of the atmospheric correction. Panels **a–d** show the MODTRAN 6 correction error and panels **e–h** show the ATCOR 4 correction error.

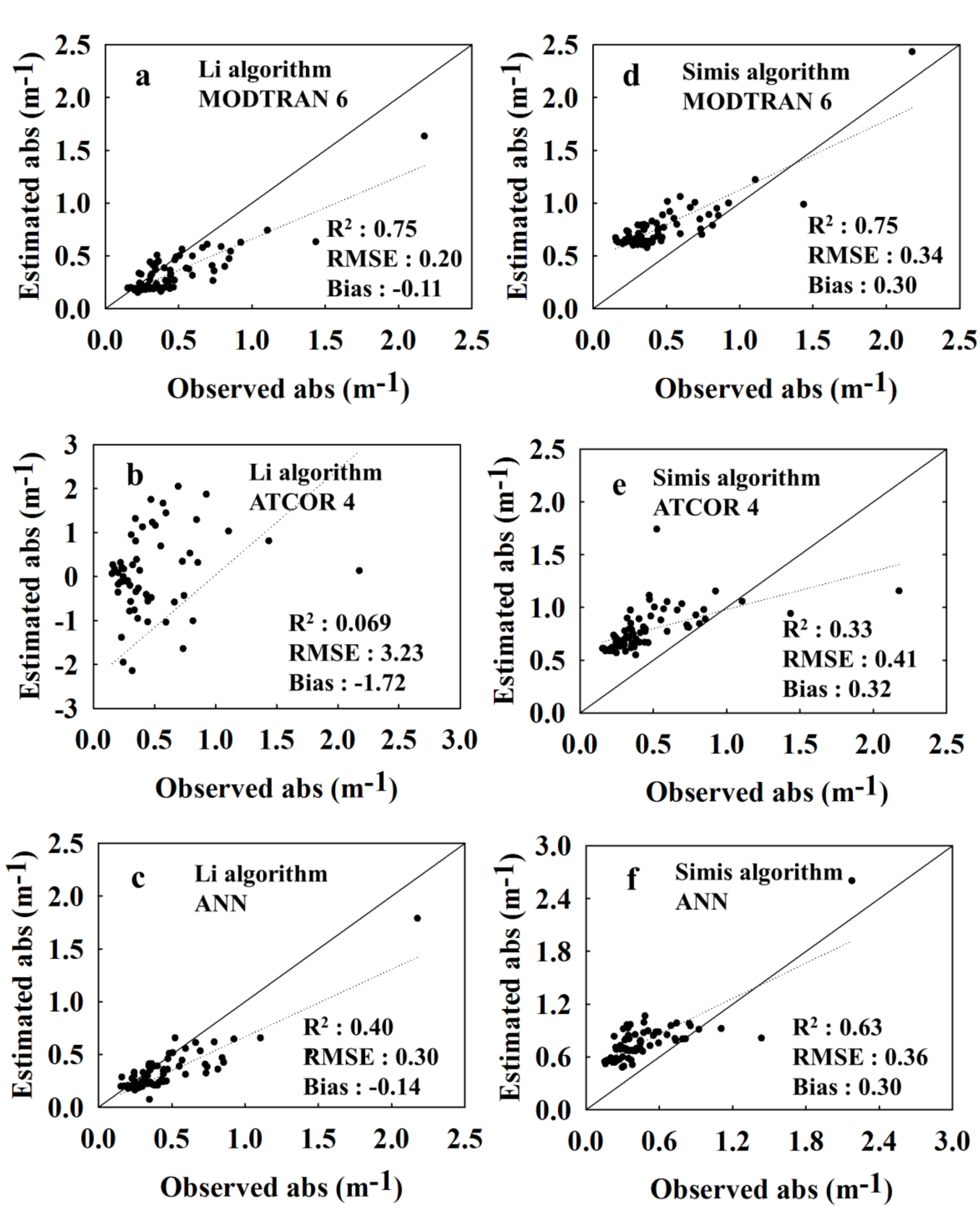

Fig. S4 Optimized absorption coefficient results of the PC algorithm with respect to in-situ and atmospheric corrected reflectance. Panels **a–c** show Li algorithm results. Panels **d–f** show Simis algorithm results. abs indicates absorption coefficient at 622nm.

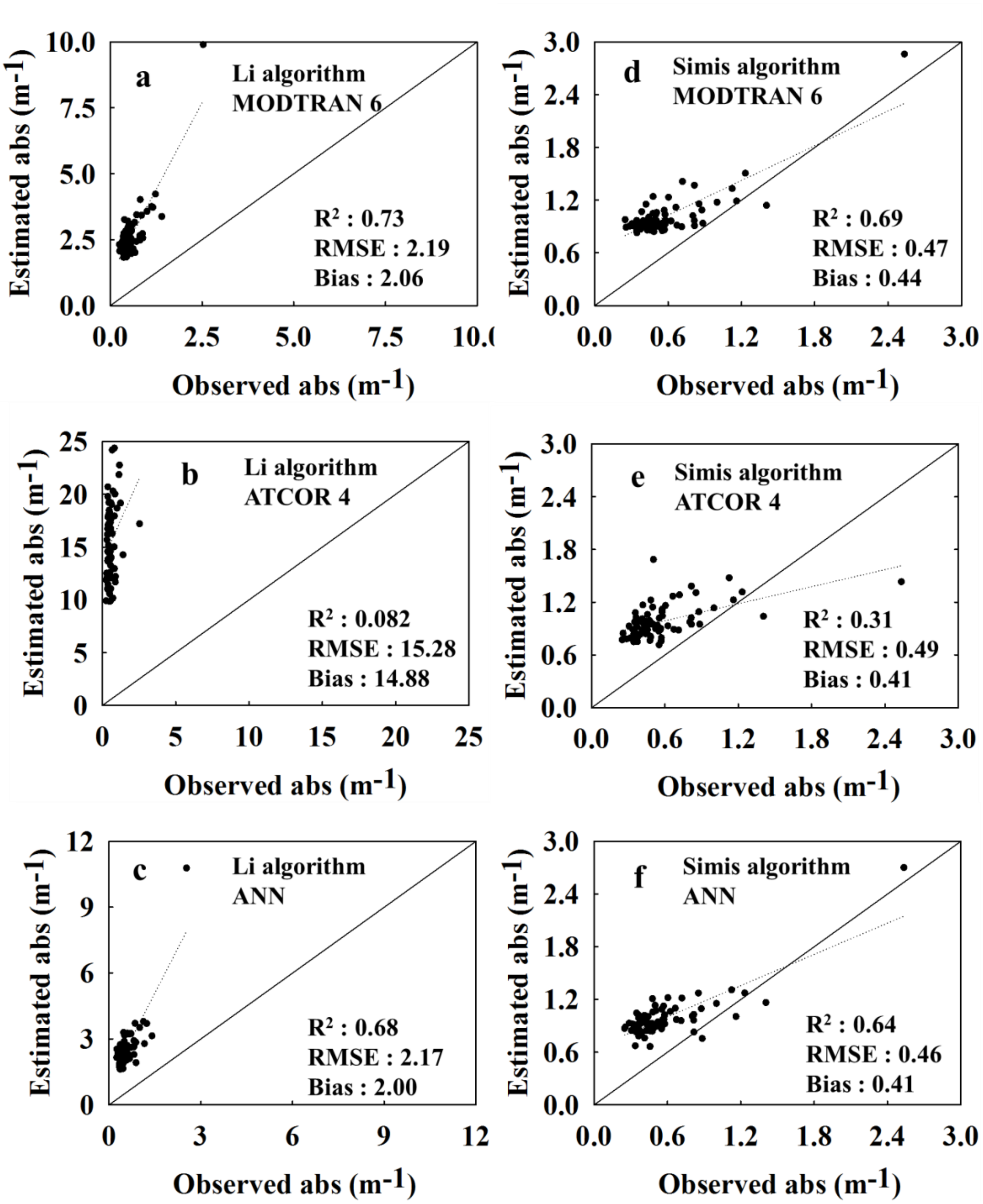

Fig. S5 Optimized absorption coefficient results of the Chl-a algorithm with respect to in-situ and atmospheric corrected reflectance. Panels **a**–**c** show Li algorithm results. Panels **d**–**f** show Simis algorithm results. abs indicates absorption coefficient at 660nm.

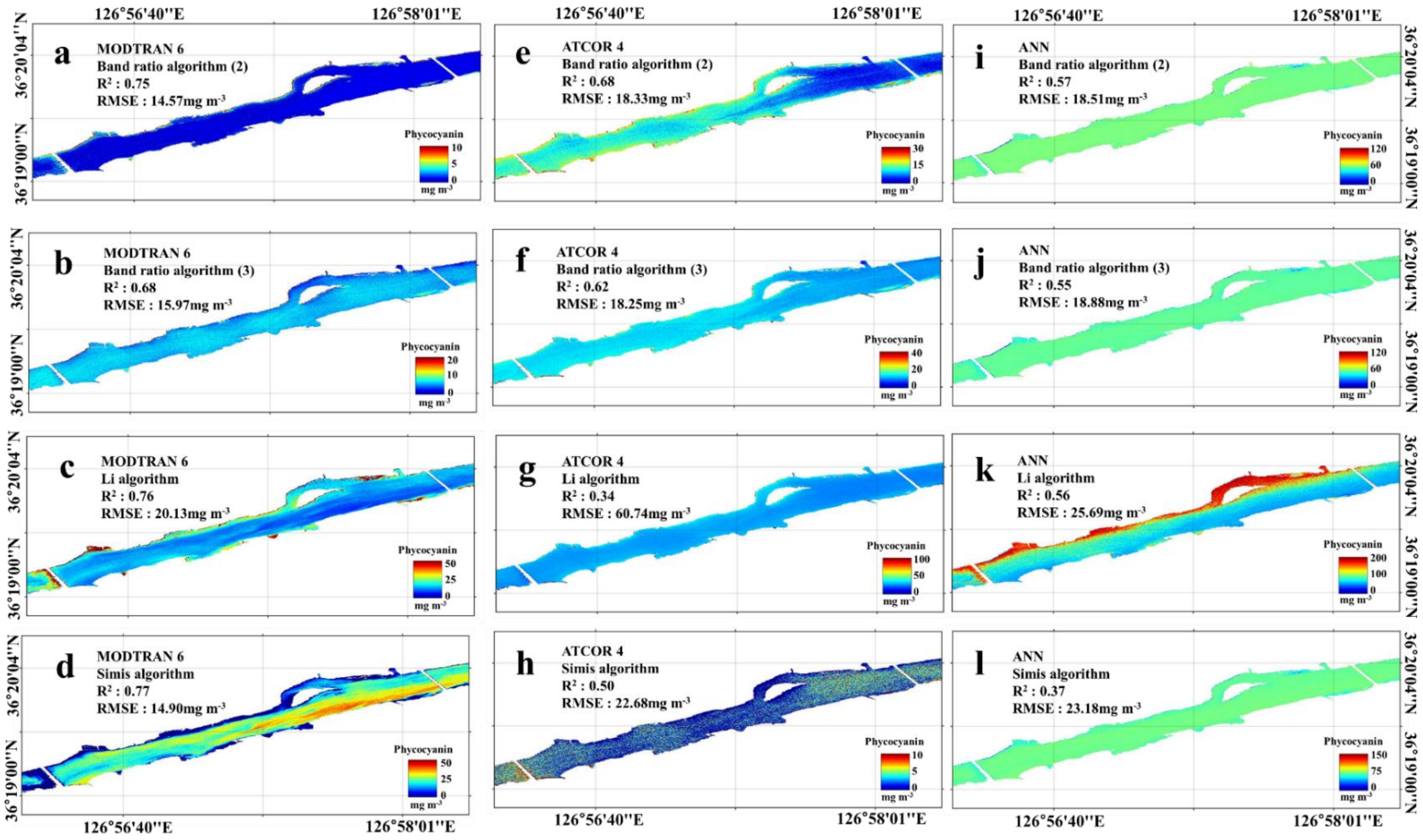

Fig. S6 *Phycocyanin* concentration images on 20 September 2016 in section 1. Panels **a–d** show the PC distribution driven by the MODTRAN 6 atmospheric correction. Panels **e–h** show the PC distribution driven by the ATCOR 4 atmospheric correction. Panels **i–l** show the PC distribution driven by the ANN atmospheric correction.

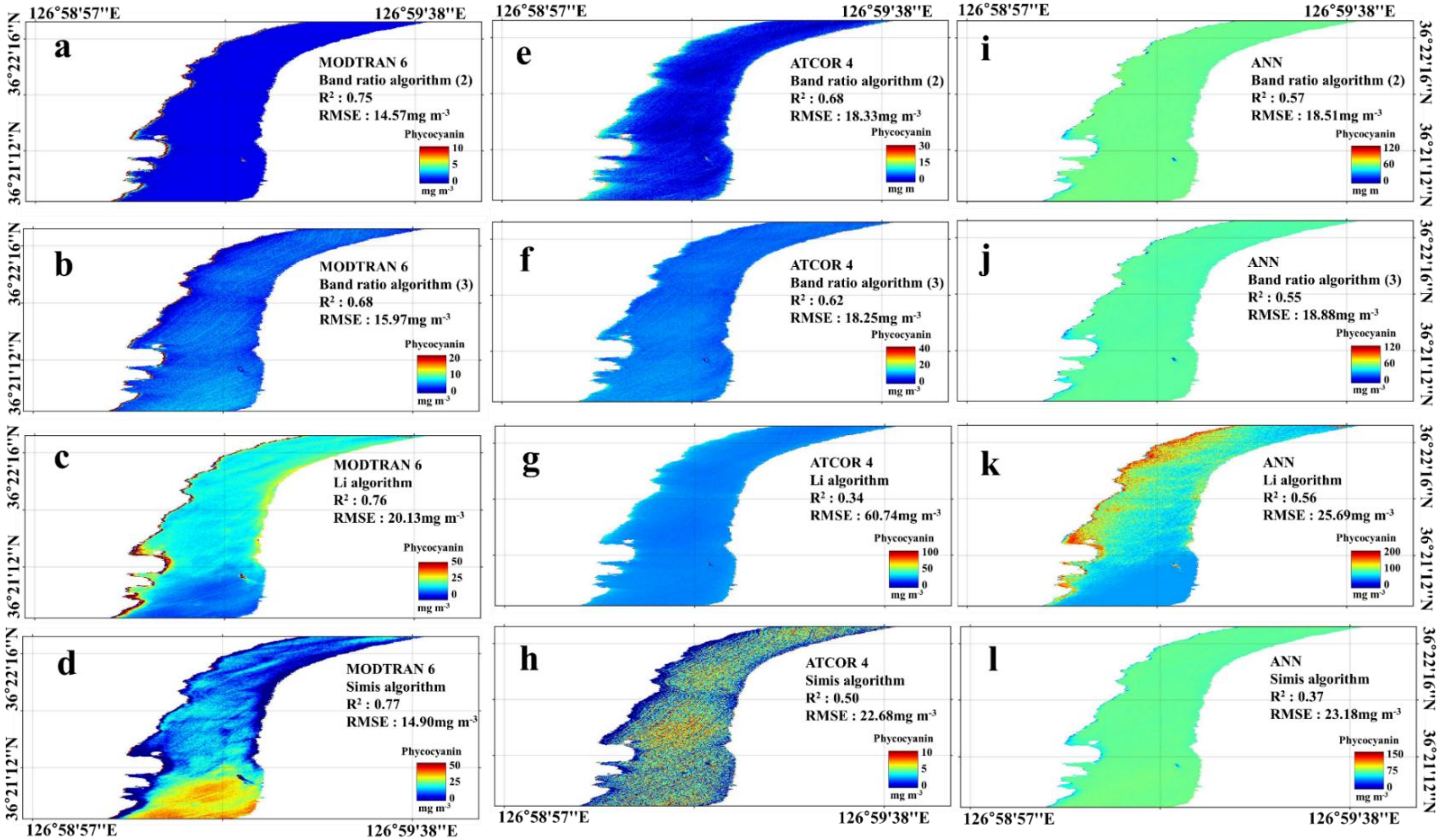

Fig. S7 *Phycocyanin* concentration images on 20 September 2016 in section 2. Panels **a–d** show the PC distribution driven by the MODTRAN 6 atmospheric correction. Panels **e–h** show the PC distribution driven by the ATCOR 4 atmospheric correction. Panels **i–l** show the PC distribution driven by the ANN atmospheric correction.

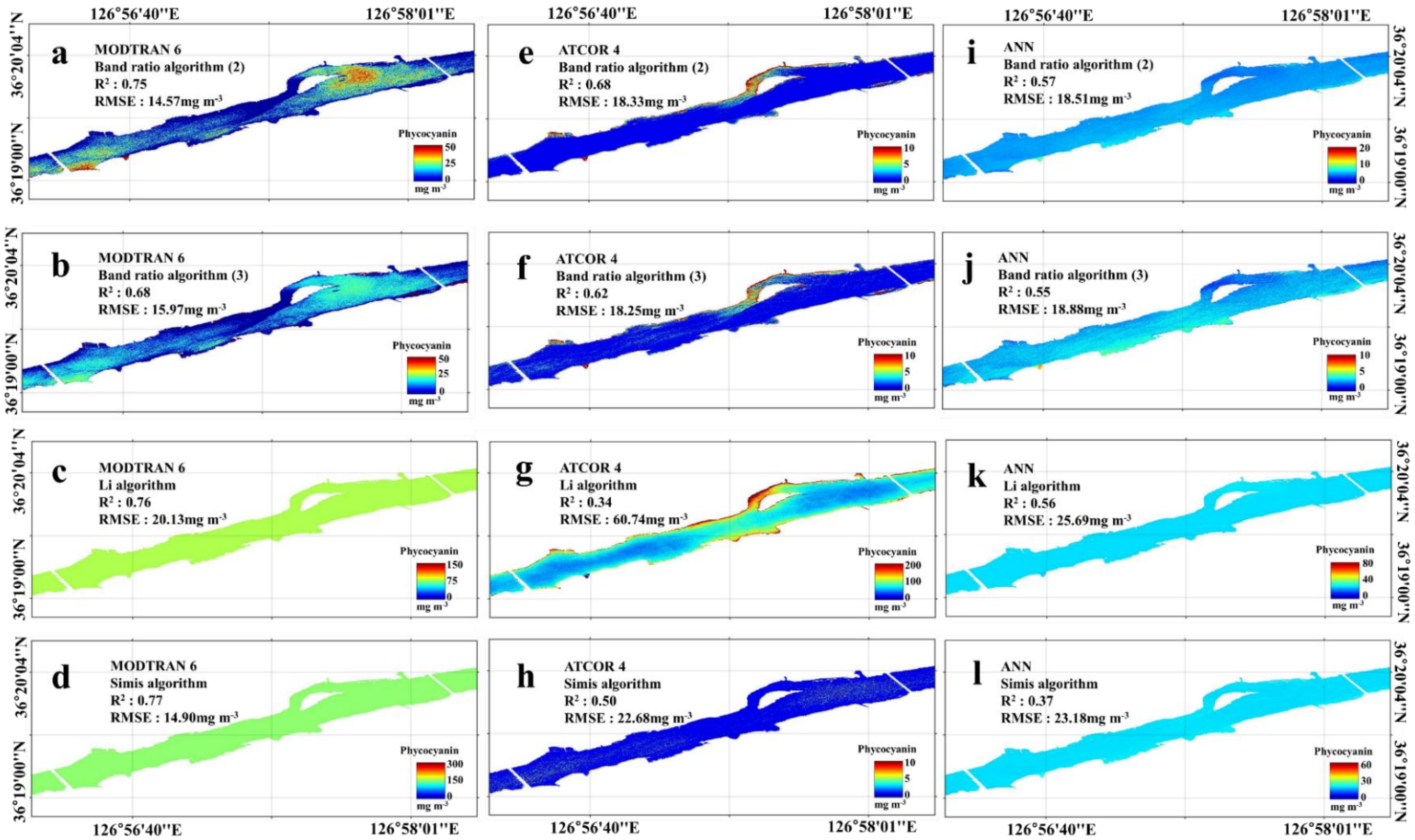

Fig. S8 *Phycocyanin* concentration images on 14 October 2016 in section 1. Panels **a–d** show the PC distribution driven by the MODTRAN 6 atmospheric correction. Panels **e–h** show the PC distribution driven by the ATCOR 4 atmospheric correction. Panels **i–l** show the PC distribution driven by the ANN atmospheric correction.

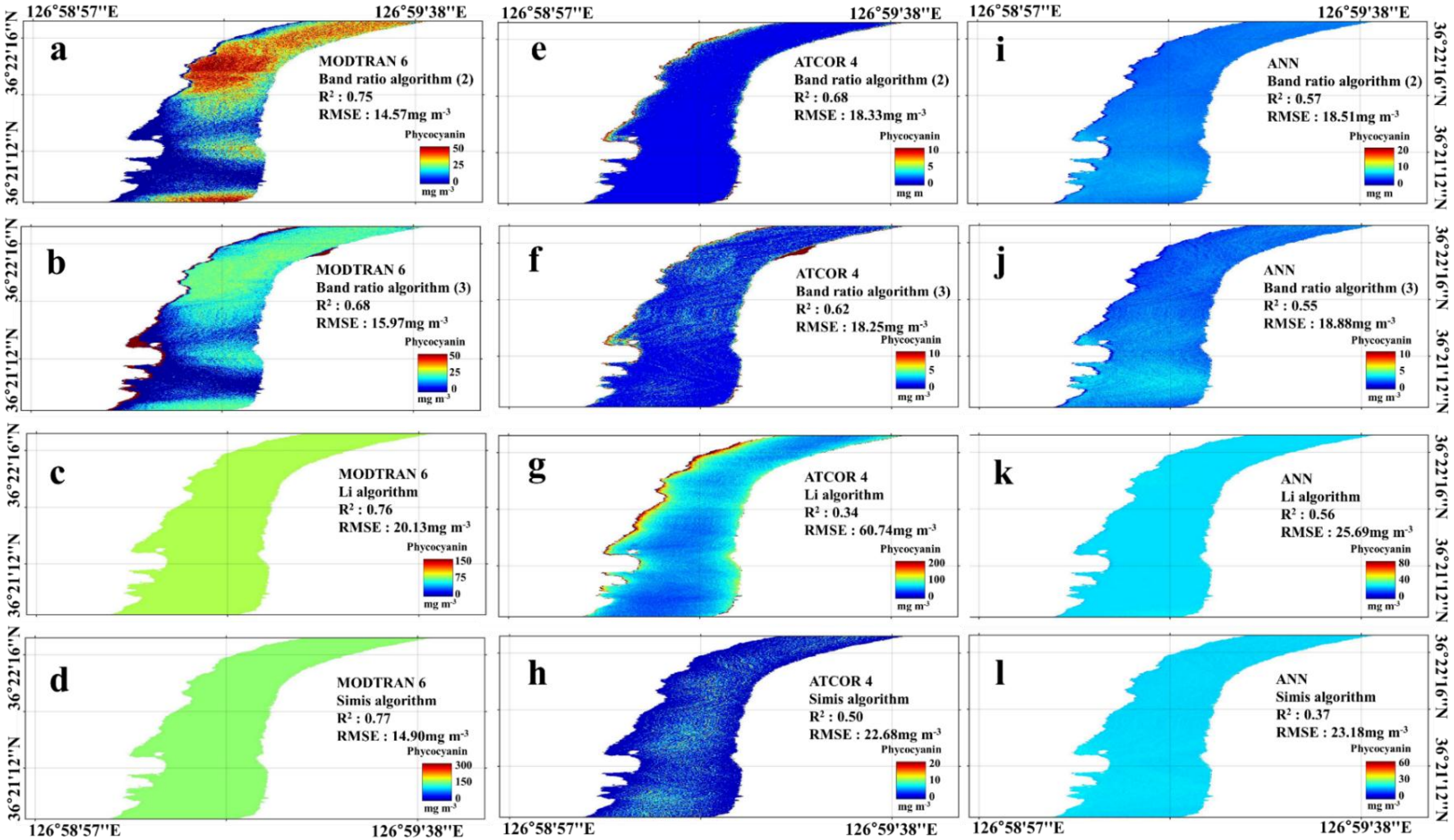

Fig. S9 *Phycocyanin* concentration images on 14 October 2016 in section 2. Panels **a–d** show the PC distribution driven by the MODTRAN 6 atmospheric correction. Panels **e–h** show the PC distribution driven by the ATCOR 4 atmospheric correction. Panels **i–l** show the PC distribution driven by the ANN atmospheric correction.

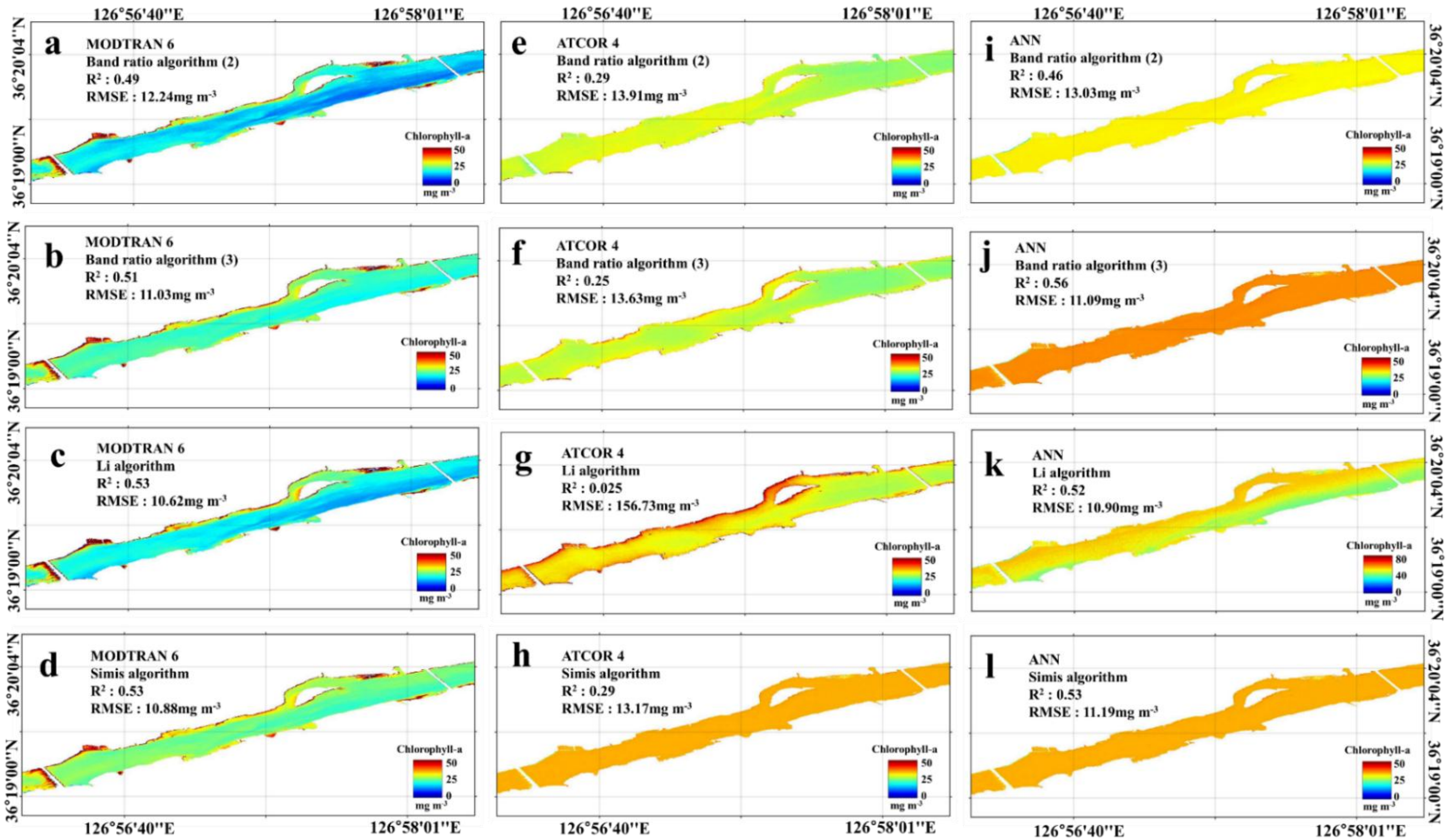

Fig. S10 *Chlorophyll-a* concentration images on 20 September 2016 in section 1. Panels **a–d** show the Chl-a distribution driven by the MODTRAN 6 atmospheric correction. Panels **e–h** show the Chl-a distribution driven by the ATCOR 4 atmospheric correction. Panels **i–l** show the Chl-a distribution driven by the ANN atmospheric correction.

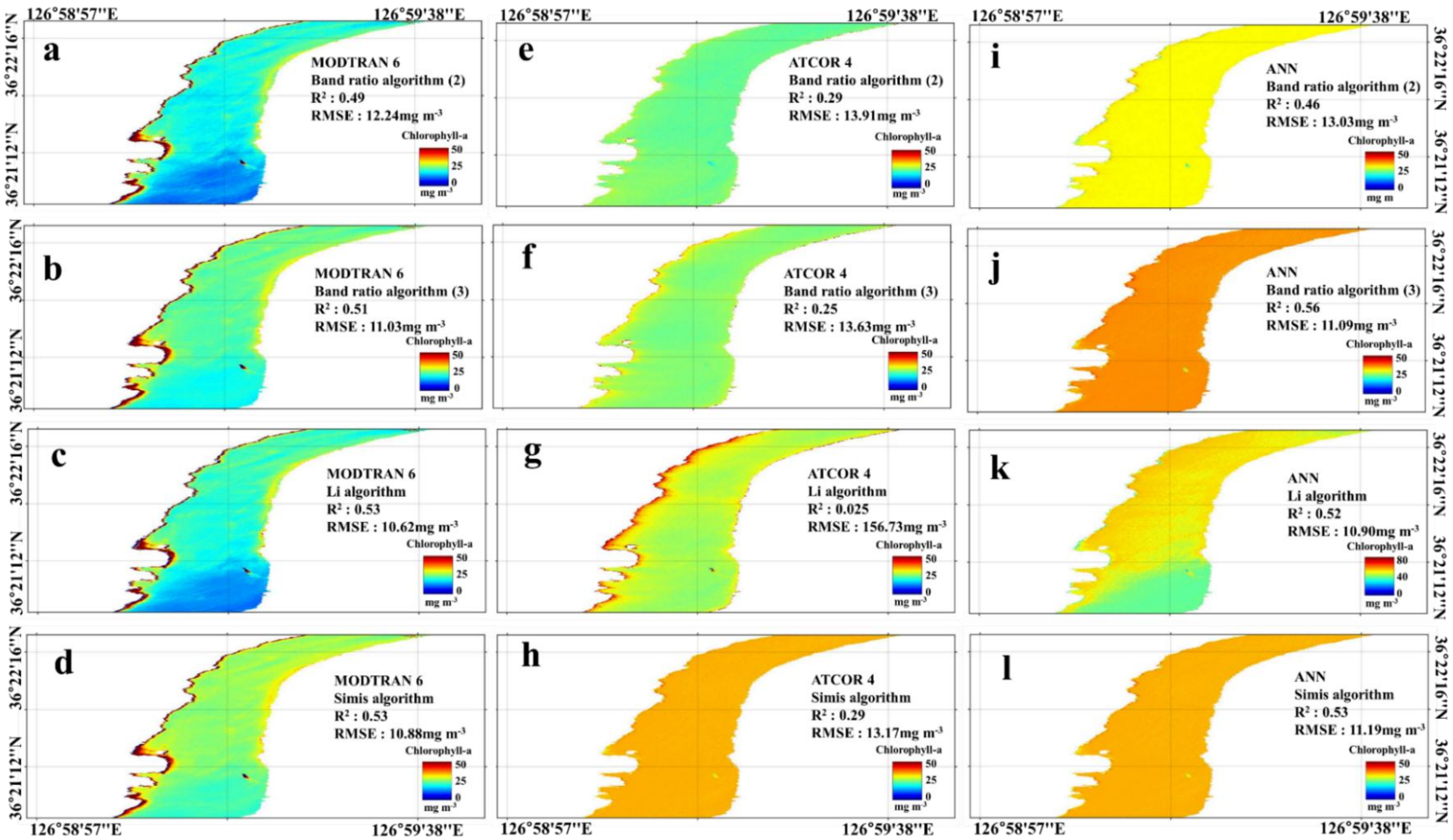

Fig. S11 *Chlorophyll-a* concentration images on 20 September 2016 in section 2. Panels **a–d** show the Chl-a distribution driven by the MODTRAN 6 atmospheric correction. Panels **e–h** show the Chl-a distribution driven by the ATCOR 4 atmospheric correction. Panels **i–l** show the Chl-a distribution driven by the ANN atmospheric correction.

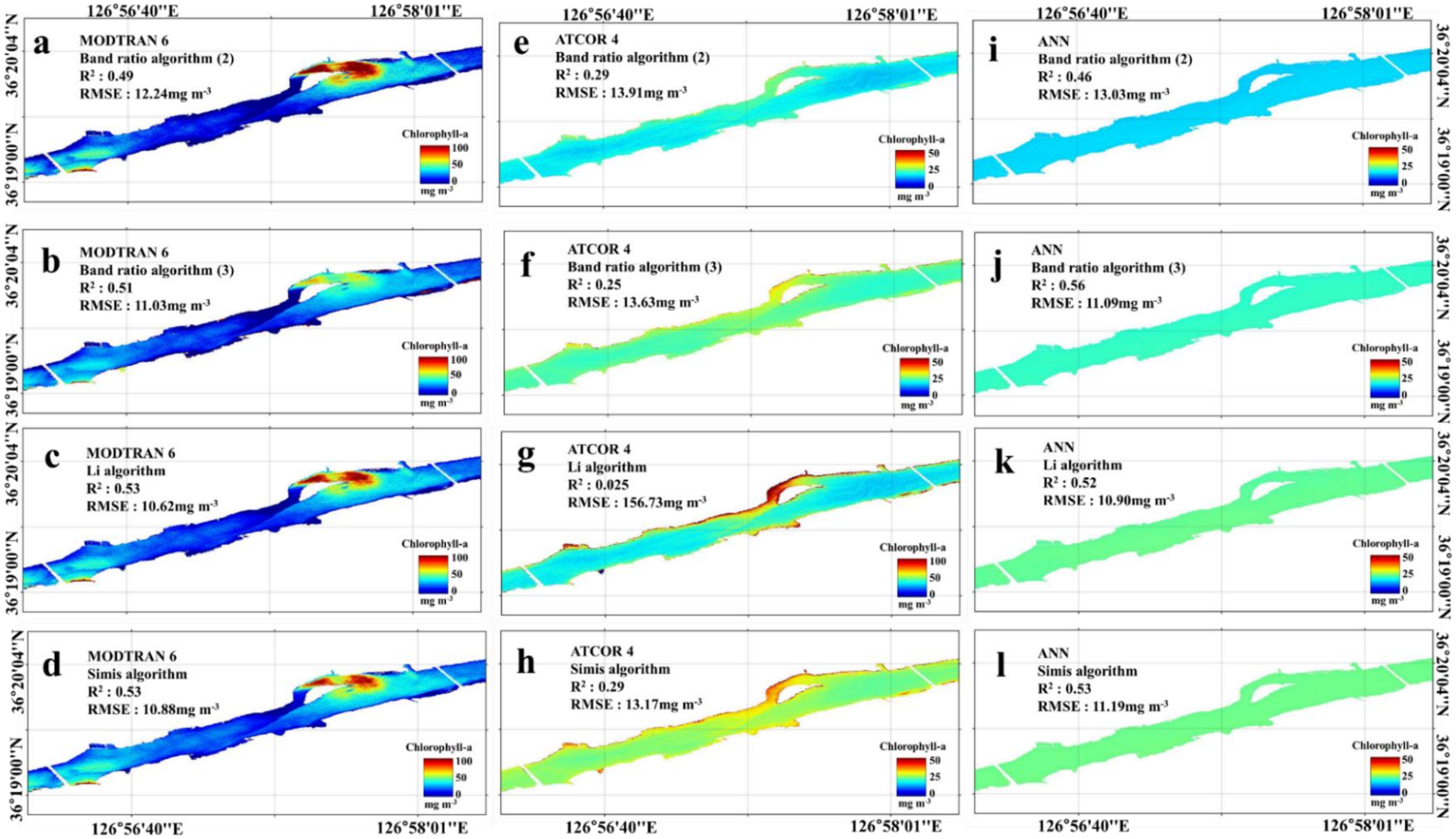

Fig. S12 *Chlorophyll-a* concentration images on 14 October 2016 in section 1. Panels **a–d** show the Chl-a distribution driven by the MODTRAN 6 atmospheric correction. Panels **e–h** show the Chl-a distribution driven by the ATCOR 4 atmospheric correction. Panels **i–l** show the Chl-a distribution driven by the ANN atmospheric correction.

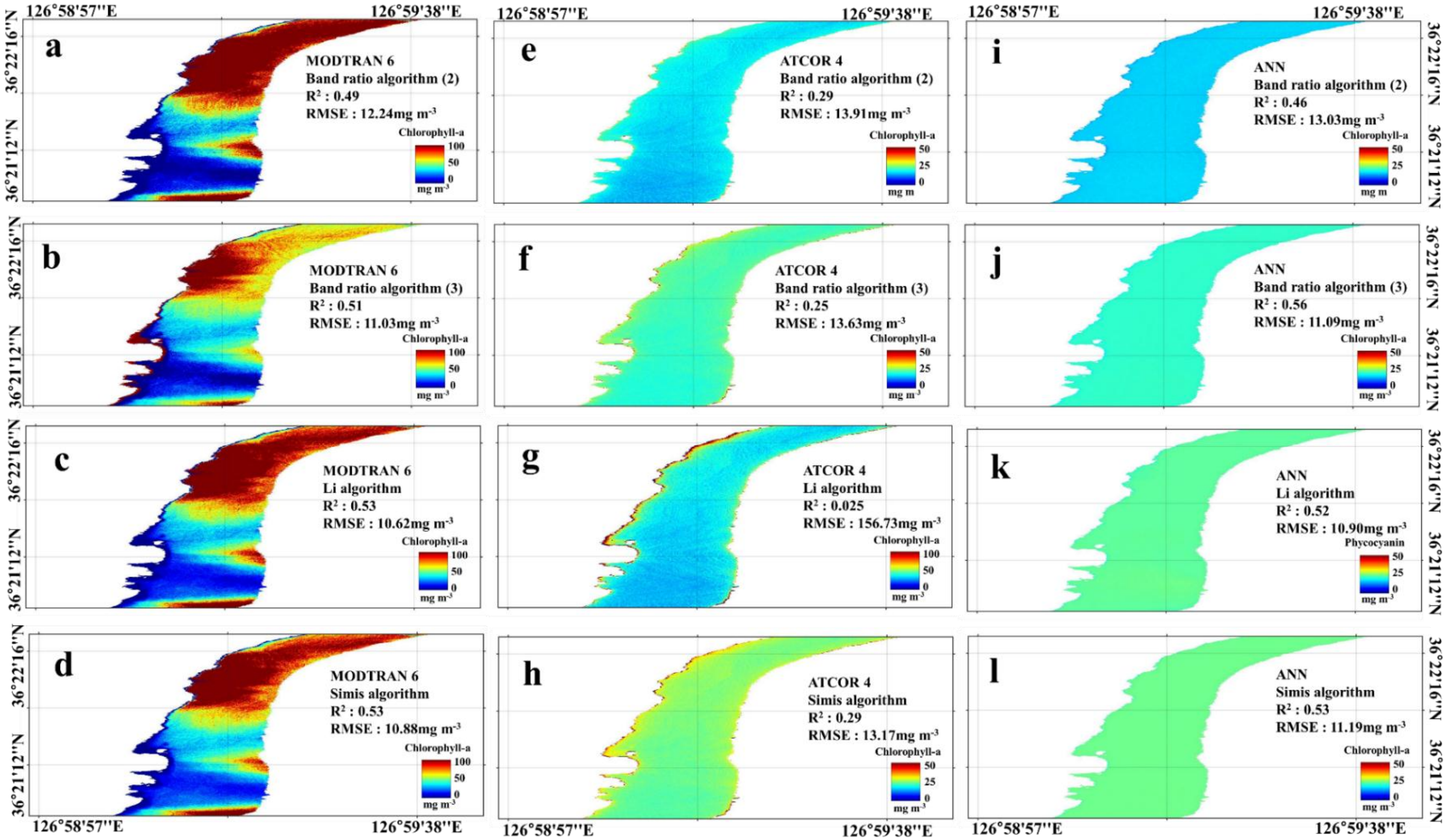

Fig. S13 *Chlorophyll-a* concentration images on 14 October 2016 in section 2. Panels **a–d** show the Chl-a distribution driven by the MODTRAN 6 atmospheric correction. Panels **e–h** show the Chl-a distribution driven by the ATCOR 4 atmospheric correction. Panels **i–l** show the Chl-a distribution driven by the ANN atmospheric correction.

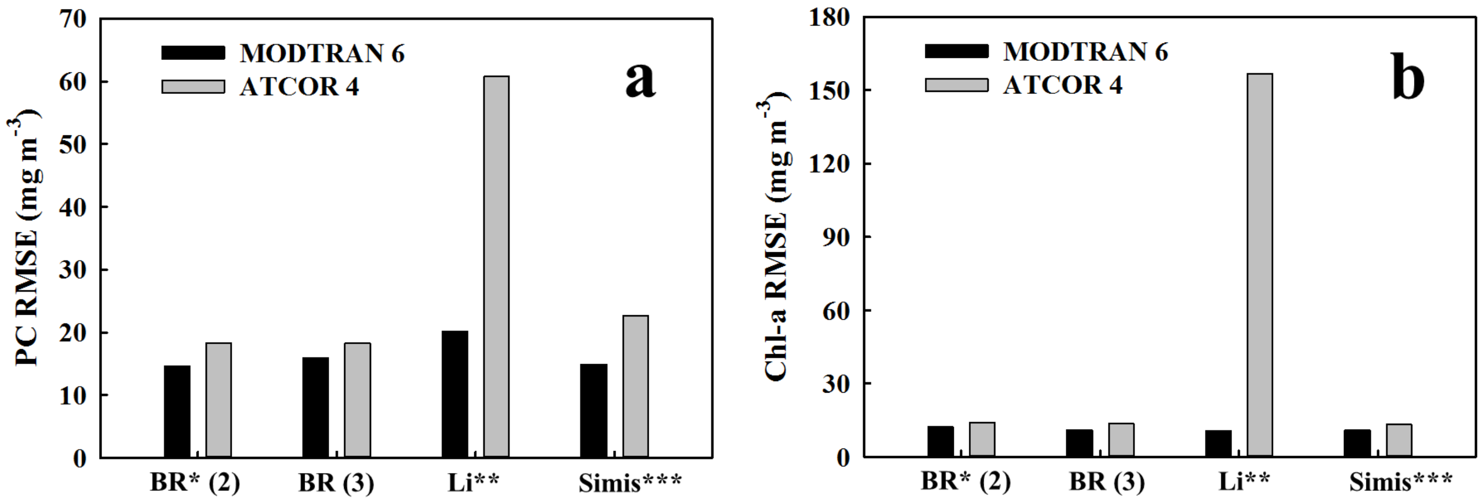

Fig. S14 Influence of atmospheric correction with MODTRAN 6 and ATCOR 4 on (**a**) the PC algorithm and (**b**) the Chl-a algorithm.* indicates the band ratio algorithm, ** indicates the Li algorithm, and *** indicates the Simis algorithm.

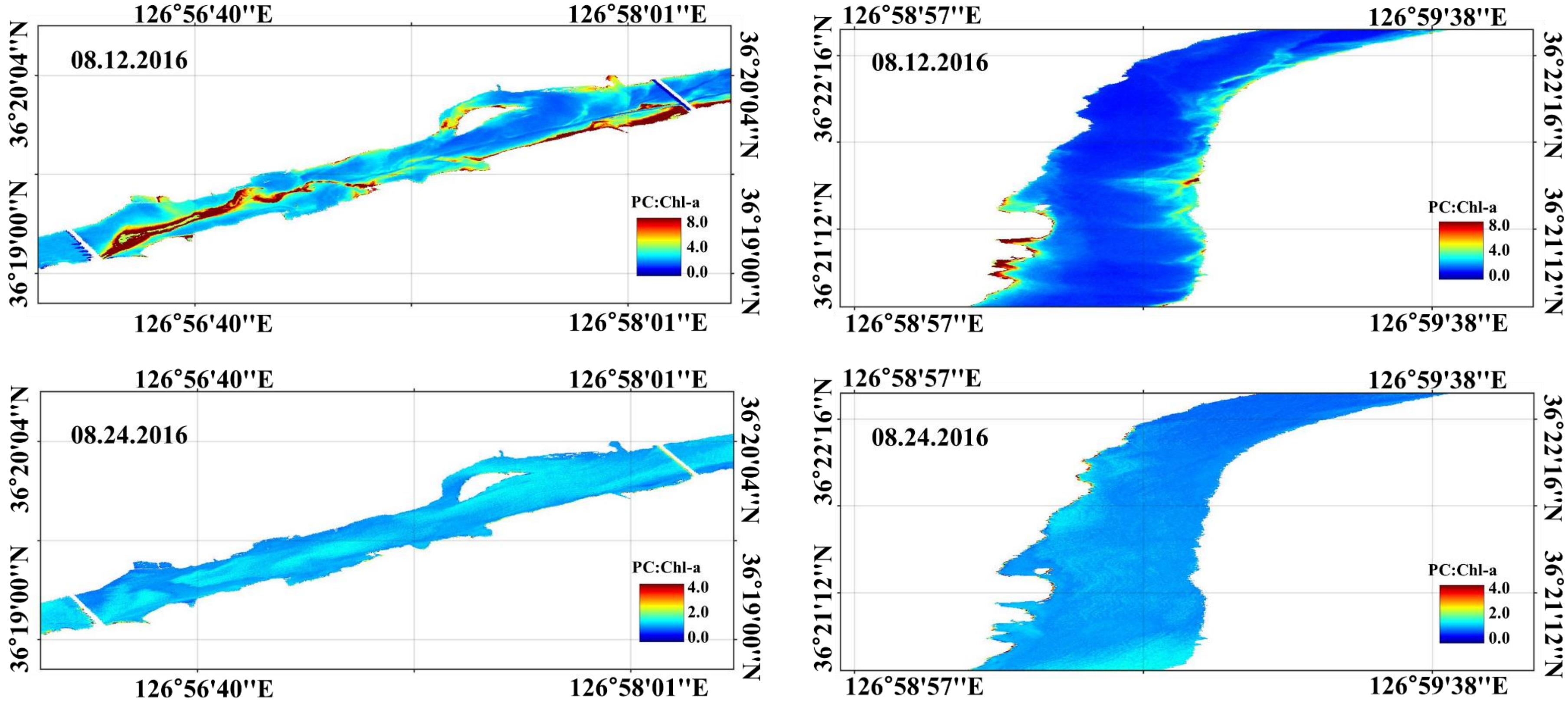

Fig S15. PC:Chl-a map estimated by Li algorithm from reflectance data corrected by MODTRAN 6 on 12 and 24 August 2016.

1. Richter, R. Atmospheric correction of dais hyperspectral image data. *Comput Geosci* **1996**, *22*, 785-793.
2. Berk, A.; Conforti, P.; Kennett, R.; Perkins, T.; Hawes, F.; van den Bosch, J. In *Modtran® 6: A major upgrade of the modtran® radiative transfer code*, Hyperspectral Image and Signal Processing: Evolution in Remote Sensing (WHISPERS), 2014 6th Workshop on, 2014; IEEE: pp 1-4.
3. Duan, S.-B.; Li, Z.-L.; Tang, B.-H.; Wu, H.; Ma, L.; Zhao, E.; Li, C. Land surface reflectance retrieval from hyperspectral data collected by an unmanned aerial vehicle over the baotou test site. *PloS one* **2013**, *8*, e66972.
4. Cho, K.H.; Sthiannopkao, S.; Pachepsky, Y.A.; Kim, K.-W.; Kim, J.H. Prediction of contamination potential of groundwater arsenic in cambodia, laos, and thailand using artificial neural network. *Water research* **2011**, *45*, 5535-5544.